NSLS-II Source Properties and Floor Layout

April 12, 2010

Contents

This document provides a summary of the current NSLS-II source and floor layout parameters. For a more complete description of the NSLS-II accelerator properties planned for NSLS-II, see the NSLS-II Preliminary Design Report at NSLS-II website. We note that this document summarizes the present status of the design, but that the design continues to be refined and that these parameters may change as part of this process.

Basic NSLS-II Storage Ring Parameters

NSLS-II is designed to deliver photons with high average spectral brightness in the 2 keV to 10 keV energy range exceeding 10^{21} ph/s/0.1%BW/mm^2/mrad^2. The spectral flux density should exceed 10^{15} ph/s/0.1%BW in all spectral ranges. This cutting-edge performance requires the storage ring to support a very high-current electron beam (I = 500 mA) with sub-nm-rad horizontal emittance (down to 0.5 nm-rad) and diffraction-limited vertical emittance at a wavelength of 1 Å (vertical emittance of 8 pm-rad). The electron beam will be stable in its position (<10% of its size), angle (<10% of its divergence), dimensions (<10%), and intensity (±0.5% variation). The latter requirement provides for constant thermal load on the beamline front ends and x-ray optics.

The optimized storage ring lattice consists of 30 DBA cells, with straight sections alternating in length between 6.6 m and 9.3 m, with low and high values of horizontal beta functions, respectively. All of the source properties described in this handout assume a fully-damped horizontal emittance of 0.55 nm-rad. This is the performance goal for the NSLS-II storage ring when operating with a full complement of insertion devices, including damping wigglers. The initial horizontal emittance of 0.9 nm-rad will be somewhat larger than this, due to the fact that only a limited number of insertion devices, including three 7 m damping wigglers, will be installed at the start of operations. The main parameters of the storage ring are summarized in Table 1.

The one sigma horizontal and vertical electron beam sizes and divergences in the center of the two types of straights, at the planned location of the 3-pole wigglers, and the range of values in the bend magnets, are given in Table 2.

Table 1. Main parameters of the NSLS-II storage ring. The high-brightness mode is envisioned to be the standard running mode of NSLS-II operations. Special run modes for pump-probe timing experiments will be explored during the NSLS-II accelerator commissioning in the early operations.

	NSLS-II high-brightness
Ring energy (GeV)	3
Ring current (mA)	500
Ring circumference (m)	792
Number of DBA cells	30
Number of 9.3 m straights	15
Number of 6.6 m straights	15
β_h in 9.3 m straights (m)	20.1
β_v in 9.3 m straights (m)	3.4
β_h in 6.6 m straights (m)	1.8
β_v in 6.6 m straights (m)	1.1
Vertical emittance (nm-rad)	0.008
Horizontal emittance (nm-rad)	0.55
RMS energy spread (%)	0.1
RMS pulse length (ps)	15-30
Time between bunches (ns)	2
Revolution period (μs)	2.64
RF frequency (MHz)	500
Number of RF buckets	1320
Number of bunches	1056
Average bunch current (mA)	0.47
Average bunch charge (nC)	1.25

Basic and Advanced Source Parameters at NSLS-II

Continuing the tradition established by the NSLS, the NSLS-II radiation sources span a very wide spectral range, from the far IR, down to 0.1 meV (equivalent to 1 cm^{-1}), to the very hard x-ray region, more than 300 keV. This is achieved by a combination of bending magnet sources (both standard gap and large gap), covering the IR, VUV, and soft x-ray range, three-pole wigglers, covering the hard x-ray range up to ~20 keV, and insertion device sources (undulators, damping wigglers, and superconducting wigglers), covering the VUV through the very hard x-ray range.

The basic parameters characterizing the NSLS-II IDs and bending magnet sources are listed in Tables 3 and 4. Table 3 illustrates the insertion devices that are currently planned. Table 4 gives the parameters for these together with the parameters of other potential insertion devices. Here, SCU stands for superconducting undulator, CPMU for cryogenic permanent magnet undulator, EPU for elliptically polarized undulator, PMW for permanent magnet wiggler, SCW for superconducting wiggler, and 3PW for three pole wiggler. All parameters are for 3.0 GeV, 500 mA operations.

It should be noted that in Table 4 the cryogenically cooled undulators and the superconducting undulators require additional R&D in areas such as cryogenic technology, in-situ magnetic field measurement instrumentation, and superconducting materials, before such devices could be constructed.

The parameters shown in Table 4 assume the baseline accelerator lattice planned for the beginning of NSLS-II operations. It is considered possible in the future to implement local short β functions in the long straights by inserting additional focusing elements in the middle of the long straights. This will allow smaller horizontal source size at the long straight sections, which may be useful for some applications, such as imaging.

Table 2. Electron Beam Size and Divergence at NSLS-II

Type of source	Low-Beta Straight Section (6.6m)	High-Beta Straight Section (9.3m)	0.4T Bend Magnet	1T Three-Pole Wiggler
σ_h (μm)	33.3	107	125	167
σ_h' (μrad)	16.5	5.1	91	98
σ_v (μm)	2.9	5.2	13.4	12.3
σ_v' (μrad)	2.7	1.5	0.80	0.82

Table 3: Currently Planned NSLS-II Insertion Devices

Type of Device	Purpose	Quantity
Damping Wiggler (DW90): 90 mm period, 1.85 T, 2 × 3.5-m long	Broadband	3
In-Vacuum Undulators (IVU):	Hard X-ray	
IVU20: 20-mm period, 1.05 T (5 mm min. gap), 3-m long		2
IVU21: 21-mm period, 0.91 T (5.5 mm min. gap), 1.5-m long, canted		1
IVU22: 22-mm period, 0.76 T (7 mm min. gap), 2 × 3-m long		1
Elliptically-polarizing undulator (EPU49): 49-mm period, 0.94 T (11.5 mm min. gap), 2 × 2-m long, optionally canted by ~0.16 mrad	Soft X-ray	1
Three-Pole Wiggler: 1.14 T peak field, 20-cm long	Broadband	1

Table 4. Basic Parameters of Current and Some Potential NSLS-II Radiation Sources for Operation at 3.0 GeV and 500 mA

	U20	U22	U17*	U14*	EPU49	DW90	SCW60	BM	3PW
Type	IVU	IVU	CPMU	SCU	EPU	PMW	SCW	Bend	PMW
Photon energy range [keV]	1.9–20	1.8-20	2.1-25	1.8-40	0.18–7	<0.01–100	<0.01–200	<0.01 – 12	<0.01 – 25
Type of straight section	Low-β	High-β	Low-β	Low-β	Low-β	High-β	Low-β		
Period length, λ_U [mm]	20	22	17	14	49	90	60		
Total device length [m]	3.0	6.0	~3	~2	4.0	7.0	1.0		0.25
Number of periods	148	270	~174	~140	2 x 39	75	17		0.5
Minimum magnetic gap [mm]	5	7	5	5	11.5	12.5	15		28
Peak field linear mode B [T]	1.03	0.74	~1.1	~1.7	0.94	1.85	3.5	0.40	1.14
Max K_y** in linear mode	1.83	1.52	~1.7	~2.2	4.34	15.7	19.6		
Peak field circular mode B [T]					0.57				
Max $K=\sqrt{2}\ K_x = \sqrt{2}\ K_y$** in circular mode					3.69				
Min. $h\nu$ fundamental [keV]	1.6	1.8	~2.1	~1.8	0.17				
Critical energy [keV]						11.1	21	2.39	6.8
Maximum total power [kW]	7.9	9.1	~9.2	~16	8.8	67	34		0.32
Horizontal angular power density [kW/mrad]						16	6.6	0.023	0.067
On-axis power density [kW/mrad^2]	66	90	~80	~105	32.8	62	25	0.088	0.26

***Requires additional R&D, with CPMU17 a near-term option and SCU14 a far-term option**

****K = 0.934 B[T] λ_u[cm]; effective K values listed**

Brightness

For many experiments, especially those involving imaging or microscopy, where the beam must be focused down to a small spot, the key figure of merit of user radiation sources is their time average brightness. This is the flux output per unit bandwidth, per unit source area, and per unit solid angular divergence. Undulators and wigglers are excellent sources of high brightness radiation. The brightness of a number of different radiation sources for NSLS-II is shown in Figure 1. For the undulators, the "envelopes" of harmonic tuning curves are shown. These "envelopes" show the variation of the peak brightness of the undulator harmonics as the magnetic field strength, and hence K parameter, is varied from K_{max}, listed for each undulator in Table 4, down to a small value.

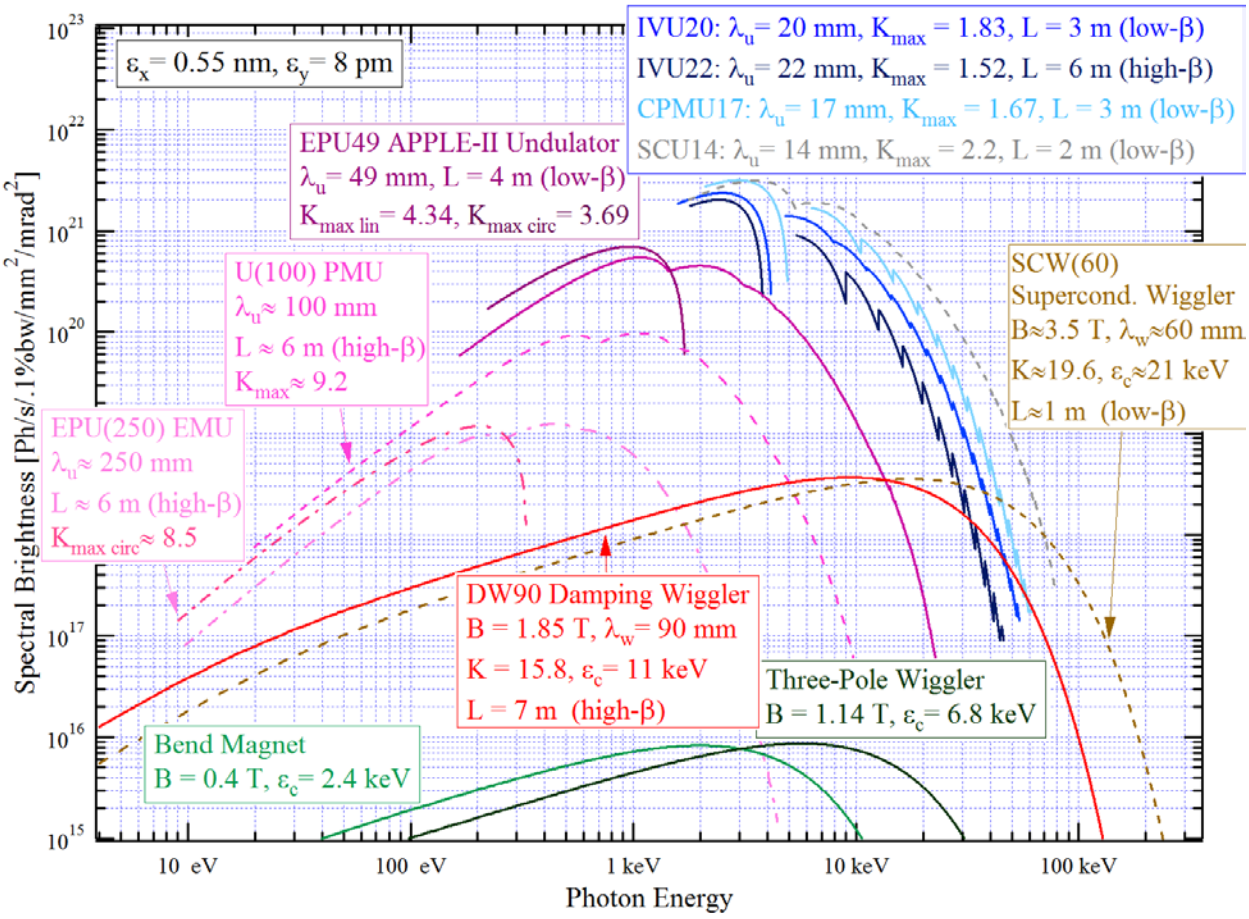

Figure 1. Brightness versus photon energy for a number of different NSLS-II radiation sources, at 3 GeV and 500 mA.

The brightness of the U14, U17, and U20 hard x-ray undulators is the highest of any of the potential devices for NSLS-II. This is due in part to the short period of these devices, thereby increasing the number of periods contributing to the flux output, and in part to the short output wavelengths compared to the soft x-ray (EPU49) and VUV (U100) undulators. For diffraction-limited undulator radiation, which characterizes a good portion of the range of these four undulators, the brightness varies inversely as the square of the output wavelength. Note that the brightness of the hard x-ray undulators (U14, U17, and U20) exceeds the 10^{21} ph/s/0.1%BW/mm^2/mrad^2 level.

The wigglers provide broadband, high brightness sources of x-ray radiation. Each of the wigglers covers nearly the entire photon energy range. The superconducting wiggler SCW60 is optimized for very high-energy x-ray work (i.e., above ~60 keV), while the damping wiggler DW90 is a high-flux, hard x-ray source with smooth spectral output extending down through the soft x-ray and VUV photon energy ranges. Figure 1 shows the brightness of the EPU49 elliptically-polarized undulators in two polarization modes: helical (or circular), shown as dotted lines, and linear, shown as solid lines. The circular polarized mode has intensity only in the fundamental and is slightly brighter than

the linearly 4 polarized mode at the same energy. It is expected that this mode will be used for all work below 2 keV for the EPU49 and below 850 eV for an EPU100 (not shown in Figure 1), unless linearly polarized light is specifically required.

NSLS-II bending magnets will be bright sources which extend from the infrared to the hard x-ray. These sources will be useful up to a few times the critical energy of 2.39 keV, i.e., up to ~10 keV. The bending magnet brightness peaks at ~2 keV, making it an ideal broadband source in the soft x-ray (0.1–2 keV) and low-energy x-ray (2–5 keV) ranges.

The 3-pole wiggler (3PW) source have a critical energy of 6 keV, making them very useful continuum hard x-ray sources up to ~25 keV. The emitted horizontal fan from these devices is 2 mrad wide.

Flux

For those experiments which do not require a very collimated and/or focused beam, the photon spectral flux is the key figure of merit. This is the number of photons per unit bandwidth per unit time. Figure 2 shows the spectral flux for the undulator sources shown in Figure 1 and Figure 3 shows the spectral flux for the wigglers and bend magnets, for which a collection angle range of 1 mrad is assumed.

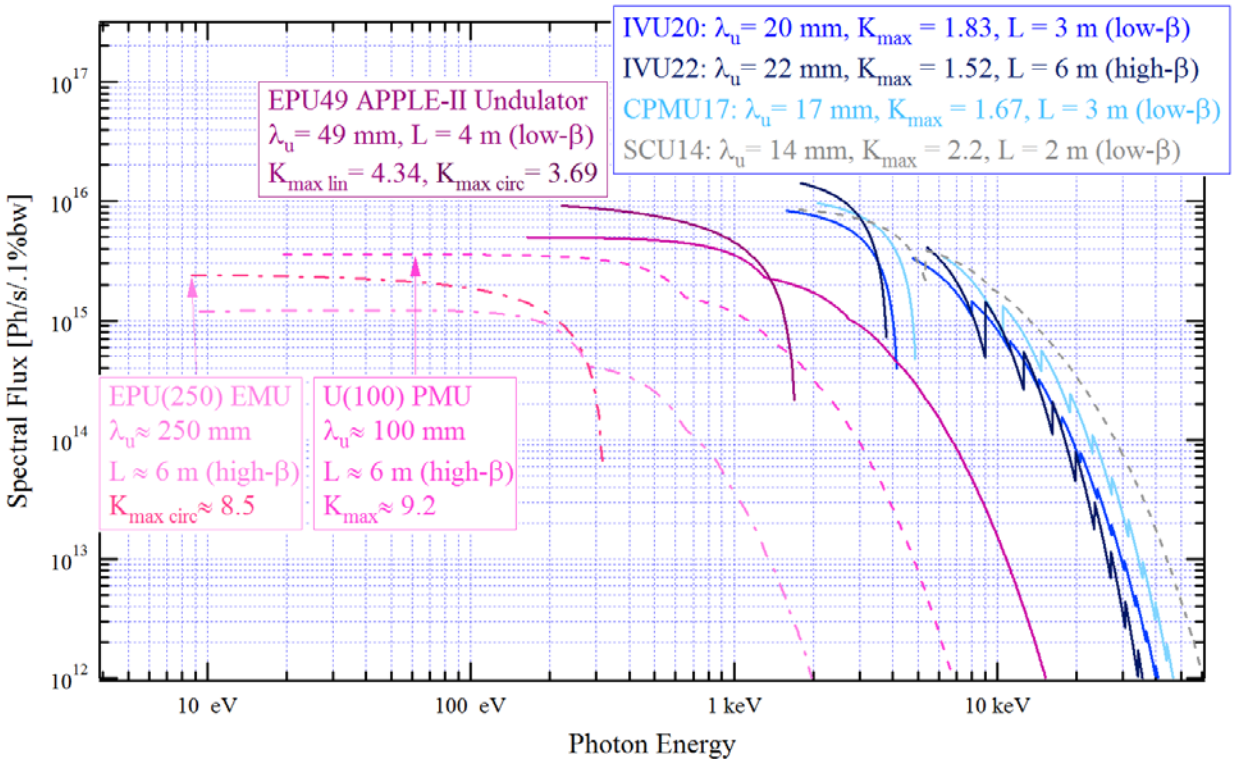

Figure 2. Spectral flux versus photon energy for a number of different NSLS-II undulators, at 3 GeV and 500 mA.

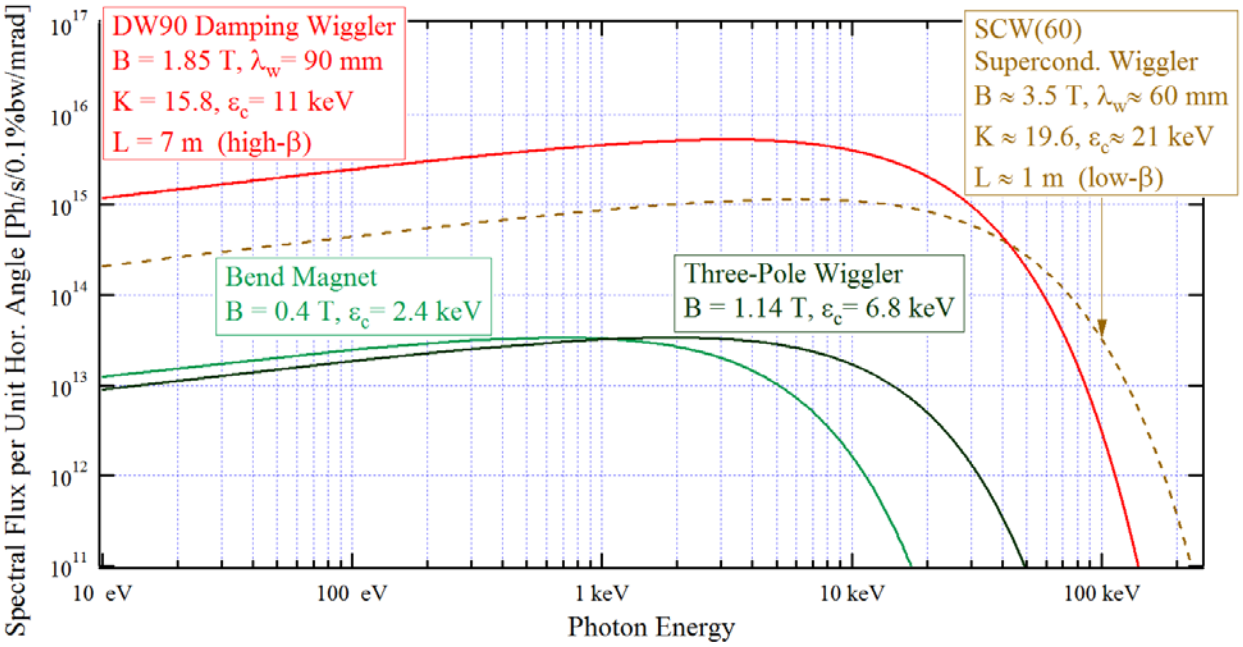

Figure 3. Spectral flux versus photon energy for a number of different NSLS-II wiggler and bend-magnet sources, at 3 GeV and 500 mA.

Photon Beam Angular Divergence

The effective RMS photon beam angular divergence of the NSLS-II undulators is shown in Figure 4 as function of photon energy. The dashed straight (on a log-log scale) lines in the right-hand graph in Figure 4 represent the "natural" photon beam angular divergence, which is the angular divergence of the "central cone" of single-electron undulator radiation at the on-axis resonant photon energy. This angular divergence is approximately given by

$$\sigma'_{nat} \approx \sqrt{\frac{\lambda}{2L}}$$

where λ is the radiation wavelength and L is the length of undulator. Finite energy spread and emittance of electron beam increase the apparent angular divergence of the photon beam. Due to the contribution of electron beam energy spread, the angular divergence of the undulator radiation beam at high harmonic numbers won't follow the above equation even if transverse emittance of the electron beam would be zero. Instead, the angular divergence of undulator radiation at n-th harmonic, taking into account the electron beam energy spread, is

$$\sigma'_n \approx \sigma'_{nat} F\left(nN\delta_e\right)$$

where δ_e is relative electron beam energy spread, N is number of undulator periods; F(x) is some monotonous increasing function: $F(0) = 1$, $F(x) > 1$ at $x > 0$. Next, the contribution of the electron beam angular divergence σ'_e to the effective photon beam divergence at n-th harmonic $\sigma'_{n\ eff}$ is taken into account by:

$$\sigma'_{n\ eff} = \sqrt{\sigma'^{2}_{n} + \sigma'^{2}_{e}}$$

The magenta and blue curves in Figure 4 show the horizontal (graph on the left) and vertical (graph on the right) effective angular divergences of the photon beam calculated for the EPU49, IVU22 and IVU20 undulators, as labeled. The solid curves correspond to exact resonant photon energies of harmonics (E_n), and the dotted curves to photon energies slightly lower than the resonant ones (by $\sim 0.4E_n/(nN)$, which provides higher flux at the harmonics). Figure 4 shows that the angular divergence of the radiation from NSLS-II undulators is close to the natural single-electron (diffraction-limited) undulator radiation divergence values in the vertical plane, and is not far from these values even in the horizontal plane, especially for the IVU22 undulator located in the high-beta straight section.

The deviation of the effective vertical angular divergence of undulator radiation at high harmonics from the corresponding natural divergence (see graph on the right in Figure 4) occurs essentially due to the contribution of the electron beam energy spread; that's why we can see distinct "divergence vs photon energy" curves corresponding to different undulator harmonics. Thus, in the NSLS-II ultra-small emittance storage ring the limiting factor governing the vertical angular divergence of the $n > 1$ undulator harmonics is the finite energy spread of the electron beam, which for the fully-damped case is $\delta_e \sim 0.001$. This effect is stronger for the hard x-ray undulators (IVU20, IVU22) than for the soft x-ray undulator (EPU49), but clearly affects both.

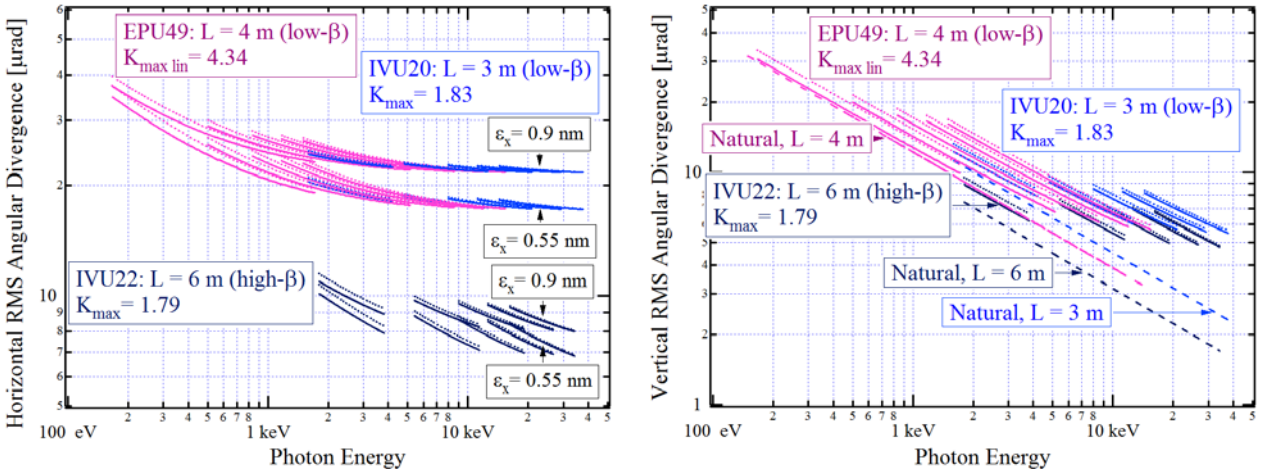

Figure 4 The angular divergence in the horizontal (left-hand graph) and vertical (right-hand graph) directions of the photon beam from the NSLS-II undulators. The straight dashed lines in the right-hand graph represent the effective angular divergences of the single-electron emission.

Photon Beam Size "at the Source"

The RMS effective photon beam sizes of the NSLS-II undulators "at the source" (i.e. near longitudinal centers of the undulators, which are assumed to be centered in straight sections) are shown in Figure 5 as functions of photon energy: the horizontal sizes are presented in the graph on the left, and the vertical sizes on the right. The lowest, straight (on a log-log graph) dashed lines in the graph on the right show the "natural" size of undulator radiation beam (emitted by one electron) at its waist. We note that due to deviation of the single-electron undulator beam from the exact Gaussian shape, the product of the "natural" undulator beam size σ_{nat} by the "natural" undulator angular divergence is $\sigma_{nat}\sigma'_{nat} > \lambda/4\pi$ (whereas for the Gaussian beam, equality holds instead of this inequality). Taking into account the first two equations in the previous section, with the contribution from electron beam energy spread, the undulator beam size at the resonant wavelength of n-th harmonic can be represented as:

$$\sigma_n = \frac{\lambda}{4\pi\sigma'_{nat}} G(nN\delta_e)$$

where $G(x)$ is some monotonous increasing function ($G(x) > 1$ at $x > 0$), which takes into account the deviation of undulator harmonics from Gaussian shape. Finally, with the contribution from finite electron beam size (σ_e), the effective photon beam size at the n-th harmonic $\sigma_{n\,eff}$ is:

$$\sigma_{n\,eff} = \sqrt{\sigma_n^{\,2} + \sigma_e^{\,2}}$$

The magenta, dark- and light-blue curves in Figure 5 show $\sigma_{n\,eff}$ (n = 1, 3, 7, 9) for the EPU49, IVU22 and IVU20 undulators respectively. The solid curves correspond to exact resonant photon energies of harmonics (E_n), and the dotted curves to photon energies slightly lower than the resonant ones (by $\sim 0.4E_n/(nN)$, which provides higher flux at the harmonics). Clearly, the undulator radiation is nearly diffraction-limited in the vertical plane over a wide photon energy range, from UV to soft x-rays. The deviation of the effective source size from the natural, diffraction-limited value is due to the contribution of both the finite electron beam size and its energy spread.

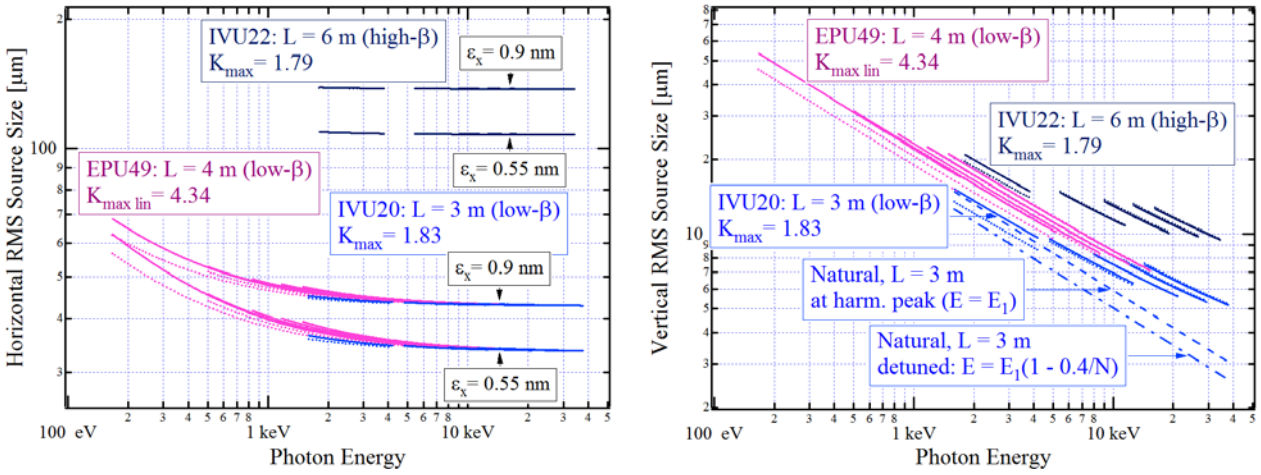

Figure 5. RMS radiation source size in the horizontal (left-hand graph) and vertical (right-hand graph) directions for NSLS-II undulators. Straight dashed lines in the right-hand graph provide the effective source size values for the single-electron emission for different undulator lengths, at the exact resonant photon energy of the fundamental harmonic, and at a slightly lower photon energy than the resonant energy.

Power

Table 4 gives the maximum total output power of the NSLS-II radiation sources, and Figure 6 below shows how the total output power of the undulator sources varies with their deflecting parameter (graph on the left), and with the corresponding photon energy of the fundamental harmonic (graph on the right). The minimal deflecting parameter value in these calculations is assumed to be K = 0.2, and the maximal K values are defined by magnetic performance of each of the undulators at their minimal vertical magnetic gap values.

The total power radiated by the undulators at their maximum K settings is in the 8–10 kW range. The total power output from the NSLS-II wigglers is higher than that of the undulators, at

nearly 65 kW for a 7 m long DW90, while that of the NSLS-II bend magnets and 3PWs is very much less, at only ~23 W and ~65W per horizontal mrad, respectively (see Table 4).

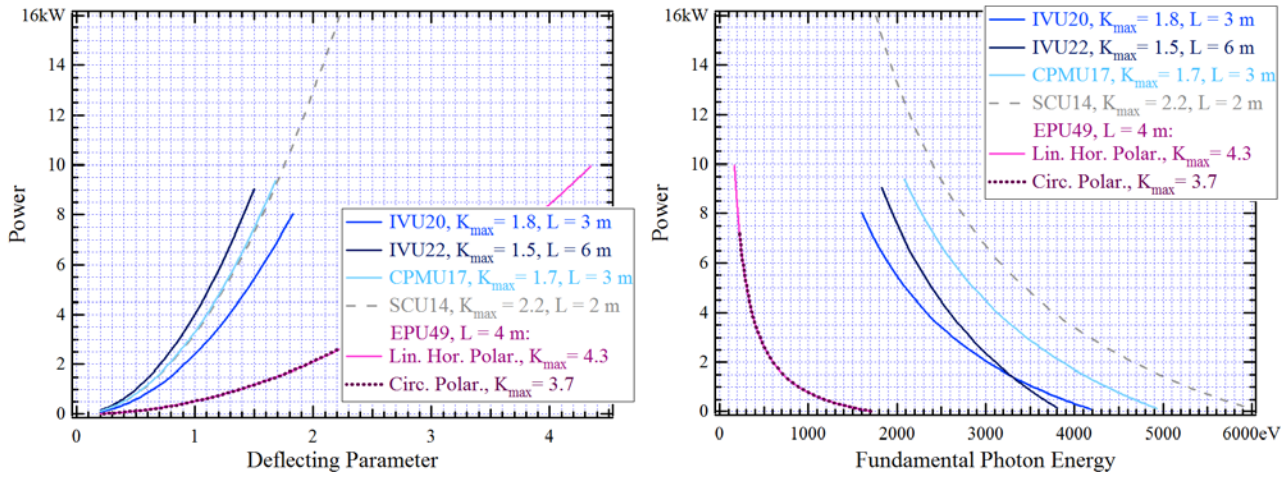

Figure 6 Total output power of various NSLS-II undulators as functions of the undulator deflecting parameter K (left) and of the fundamental photon energy (right).

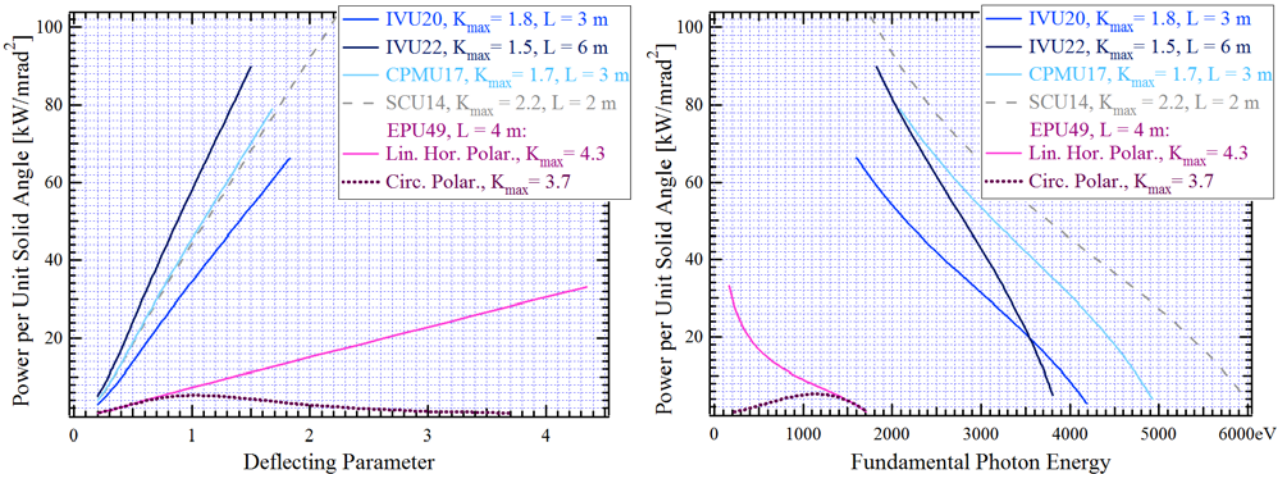

Figure 7. Power per unit solid angle emitted by various NSLS-II undulators along the electron beam axis, as function of the deflecting parameter (left) and of the output fundamental photon energy (right).

Table 4 gives, among other parameters, the maximum on-axis angular power density of the NSLS-II radiation sources. The left graph in Figure 7 shows how the maximum on-axis angular power density of the undulators varies as their deflecting parameter changes from K_{min} (taken to be ~0.2) to K_{max} (which is defined by magnetic performance at minimal gap). In the graph on the right, the undulator angular power density is plotted as function of the fundamental photon energy (the energy of n-th harmonic is *n* times that of the fundamental). The maximum undulator angular power density radiated by the undulators at their maximum K settings varies from 30 to 90

kW/mrad^2. The wiggler angular power density output is similar, in the 25–60 kW/mrad^2 range, while the bend magnet and 3PW values are again very much less, at 88 W/mrad^2 and 260 W/mrad^2, respectively.

Figure 7 shows that the EPU49 output angular power density in the "on-axis" direction in circular polarization mode is much lower than in the linear polarization mode, and has different dependence on K. This is primarily because in circular polarization mode, only the fundamental UR harmonic is emitted on the electron beam axis; whereas the higher harmonics are emitted into angular "rings" off the electron beam axis. The lower output power density in circular polarization mode simplifies the design and operation of high energy-resolution beamlines by reducing the thermal deformations of the optical elements.

In practice, it is often necessary to know not only the power density in the "on-axis" direction, but also the power distribution "off the axis" as a function of the horizontal and vertical angles. Such distributions, calculated for various NSLS-II undulators at minimal gap (maximal K values), and for the damping wiggler, are shown in Figure 8.

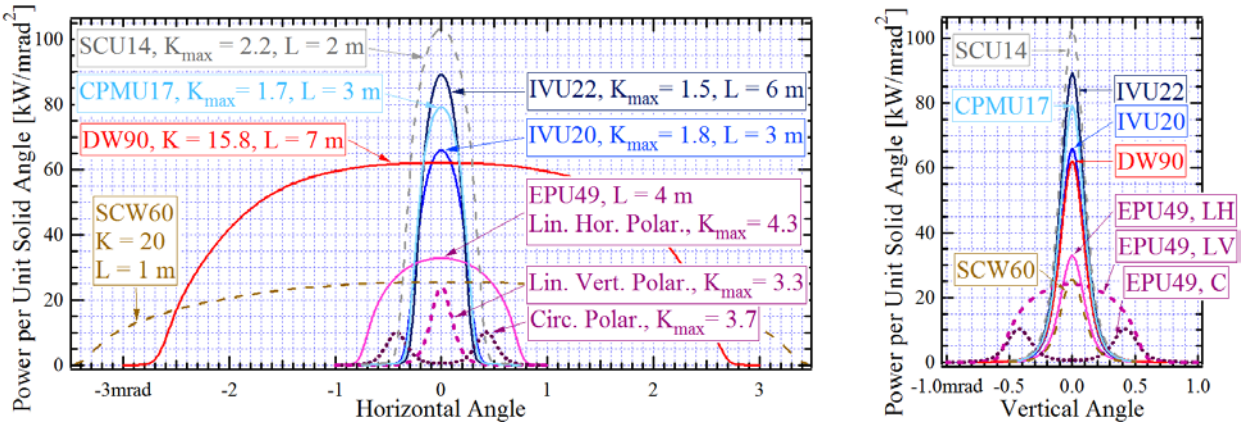

Figure 8. Radiation power per unit solid angle from various NSLS-II undulators and damping wiggler at different horizontal (left) and vertical (right) observation angles in the horizontal and vertical median planes respectively, for the maximal magnetic field.

Infrared Sources

Figure 9 shows the NSLS-II brightness for the very far-, far- and mid-infrared spectral ranges, for both the standard gap and large gap (90 mm) dipoles and associated extraction chambers. The brightness curves are compared to that of the existing NSLS VUV/IR ring. In the mid-infrared range from 1 to 20 micron wavelengths, the standard-gap dipole and extraction optics are sufficient. In this range, the lower emittance of NSLS-II results in up to an order of magnitude greater brightness compared to NSLS. In the very far-infrared range, especially for wavelengths greater than 1 mm, the large-gap dipole and extraction optics become essential in preserving brightness, and can be seen to produce spectral brightness equal to the world class performance of the NSLS very far-IR

ports. In this wavelength range, the standard-gap dipole and extraction suffers both from waveguide cutoff effects and limitations from small horizontal collection fan angle.

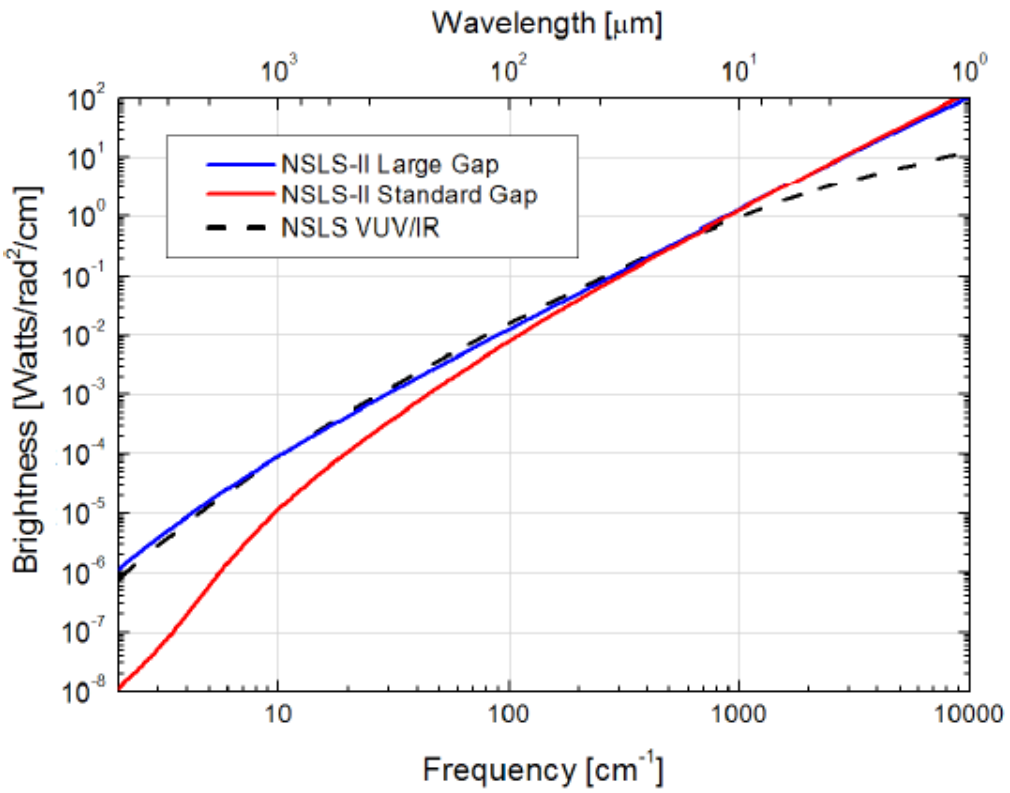

Figure 9. Brightness of NSLS-II infrared sources.

Distribution of Sources Available for User Beamlines

NSLS-II will accommodate at least 58 beamlines for user experiments, distributed by type of source as follows:

- 15 low-beta ID straights for user undulators or superconducting wigglers
- 12 high-beta ID straights for either user undulators or user damping wigglers
- 31 BM ports providing broadband sources covering the IR, VUV, and soft x-ray ranges. Any of these ports can alternatively be replaced by a 3PW port covering the hard x-ray range.
- 4 BM ports on large gap (90 mm) dipoles for very far-IR

Multiple (possibly two) IDs may be installed in a single straight section, and these IDs may be canted by a horizontal angle of 0-2 mrad. Each 7 m long damping wiggler is made of two 3.5 m long wigglers, which can also be canted. In the canted case, the total active ID length is reduced by the size of the canting magnet.

Floor Layout

The standard floor space available for beamline components, ranging from just outside the ring shield wall to the exterior walkway, is given in Table 5 below. Note that these dimensions vary depending on the type of source and the type of cell (low-β or high-β ID straight). As shown in Figure 10 below, the experimental floor radial width of the majority of the sectors has an extended value, with only the sectors near the main entrance and near the main loading dock having a somewhat smaller standard value. Beamlines up to 72 m long can be built within the ring building in sectors with the extended experimental floor width, as compared to 66 m long beamlines in sectors with the standard floor width. Extra-long (>200 m) beamlines extending beyond the exterior walkway with endstations located outside the ring building can also be considered.

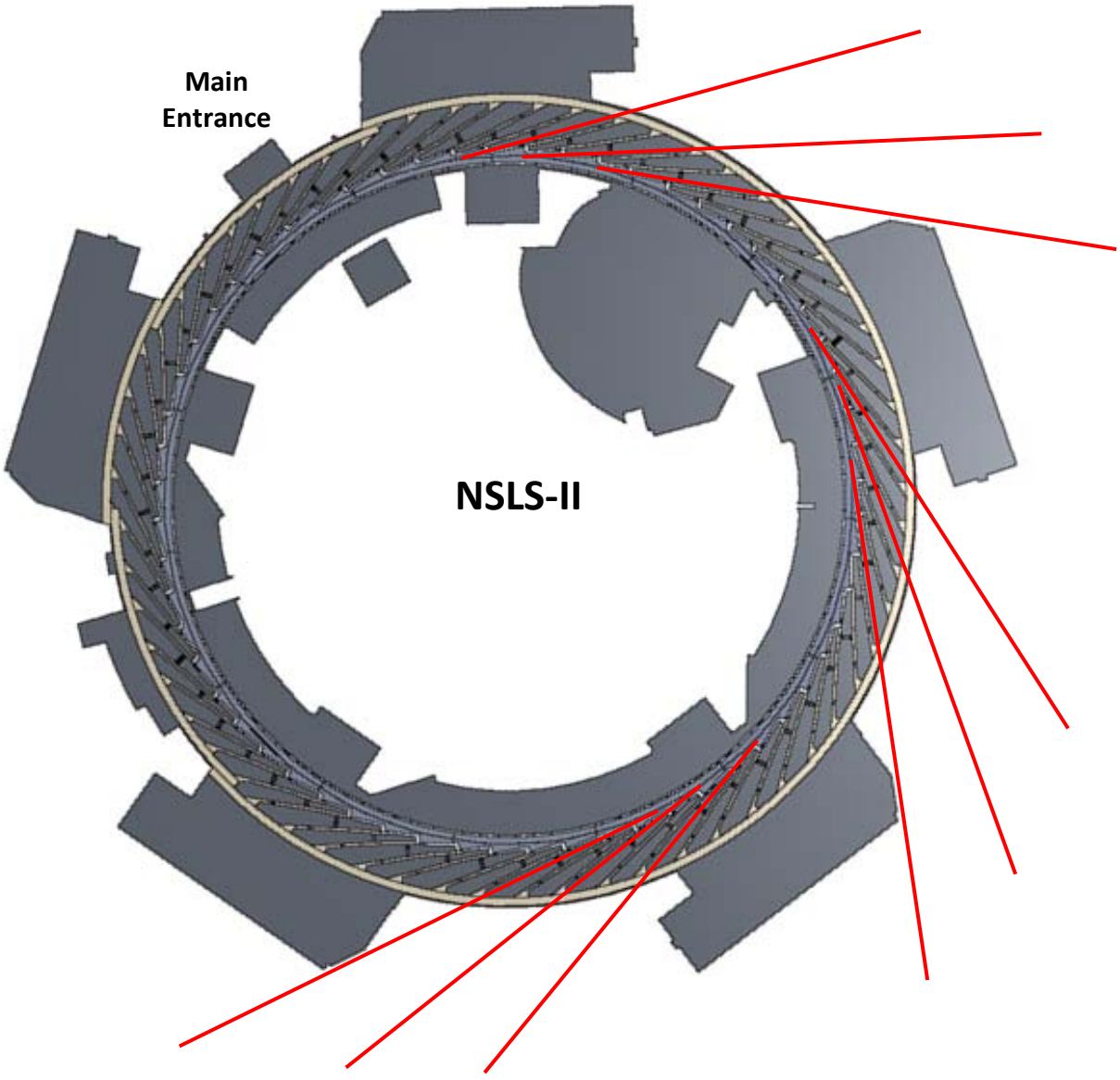

Figure 10. Experimental floor space in the NSLS-II ring building. The red lines indicate possible long beamlines extending outside of the ring building.

Table 5. Floor layout dimensions for NSLS-II beamlines located at different sources

Source description	Distance from source to downstream face of shield wall (m)	Distance from source to walkway on extended floor (m)	Distance from source to walkway on standard floor (m)
High-β ID straight (even sector)	26.717	73.713	67.379
Low-β ID straight (odd sector)	25.468	73.49	67.135
3PW downstream of high-β ID	23.543	69.94	63.586
3PW downstream of low-β ID	24.828	71.22	64.834
BM downstream of high-β ID	23.189	69.874	63.487
BM downstream of low-β ID	24.471	71.127	64.742